Collimated LED Array With Mushroom-Cap Encapsulation for Near-Eye Display Projection Engine

Enguo Chen, *Member, IEEE*, Ziming Yao, Zhengui Fan, Wenzong Lai, Tao Liang, Qun Yan, *Member, IEEE*, Tailiang Guo, and Chao Ping Chen, *Member, IEEE*

(Invited Paper)

***Abstract*—As metaverse continues to evolve, near-eye display technologies are increasingly focused on achieving compactness, lightweight, and high brightness design. Self-emitting projection sources have garnered significant attention due to their potential to meet these requirements. However, current projection sources typically exhibit a Lambertian-like divergence angle, leading to challenges in miniaturization and substantial energy loss. In response to these issues and inspired by the shape of "mushroom cap", this paper proposes a collimated light-emitting diode array encapsulated with mushroom-cap optical units for near-eye display projection engine. The study discusses the optimal parameters for the limited diode spacing and validates these parameters through both simulation and experimental results. The mushroom-cap optical units effectively harness the emitting energy, confining the full width at half maximum of Lambertian sources within the $\pm 10^{\circ}$ range, while enhancing the central light intensity by 80%. The built experimental prototype demonstrates a significant enhancement in projection quality and visibility. This design holds promise for ultra-small self-emitting projection engines, offering robust support for the high performance and lightweight design of near-eye display devices.**

***Index Terms*—Light-emitting diode, collimation, projection engine, near-eye display.**

Manuscript received 12 January 2024; revised 6 March 2024; accepted 6 March 2024. Date of publication 18 March 2024; date of current version 1 April 2024. This work was supported in part by the National Key Research and Development Plan of China under Grant 2022YFB3603503, in part by the National Natural Science Foundation of China under Grant 62175032, in part by the Fujian Science & Technology Innovation Laboratory for Optoelectronic Information of China under Grant 2020ZZ111, and in part by the Natural Science Foundation of Chongqing under Grant cstc2021jcyj-msxmX1136. *(Corresponding author: Chao Ping Chen.)*

Enguo Chen, Qun Yan, and Tailiang Guo are with the National and Local United Engineering Center of Flat Panel Display Technology, College of Physics and Information Engineering, Fuzhou University, Fuzhou 350108, China, and also with the Fujian Science and Technology Innovation Laboratory for Optoelectronic Information of China, Fuzhou 350108, China (e-mail: ceg@fzu.edu.cn; qunfyan@gmail.com; gtl@fzu.edu.cn).

Ziming Yao, Zhengui Fan, Wenzong Lai, and Tao Liang are with the National and Local United Engineering Center of Flat Panel Display Technology, College of Physics and Information Engineering, Fuzhou University, Fuzhou 350108, China (e-mail: 1258537269@qq.com; 1003979968@qq.com; laiwz1995@qq.com; lt_fzu@126.com).

Chao Ping Chen is with the Smart Display Lab, Department of Electronic Engineering, Shanghai Jiao Tong University, Shanghai 200240, China (e-mail: ccp@sjtu.edu.cn).

Color versions of one or more figures in this article are available at https://doi.org/10.1109/JSTQE.2024.3375929.

Digital Object Identifier 10.1109/JSTQE.2024.3375929

I. Introduction

In recent years, next-generation near-eye display devices such as augmented reality (AR) and virtual reality (VR) have emerged as focal points in both research and industry [1]. These innovative display devices are poised to propel us into a new era known as metaverse, surpassing the era of mobile internet [2], [3], [4], [5], [6]. Compared to traditional devices, these next-generation display devices demand denser pixels, brighter light sources, and an overall lighter and more compact form factor [7]. This places higher requirements on light sources and imaging systems, prompting researchers to seek and develop advanced technologies capable of meeting these conditions. Traditional display technologies, e.g., liquid crystal display, rely on external components such as the backlights and color filters [8], [9]. The presence of these components not only occupies valuable space but also necessitates complex and bulky supporting structures for their operation [10]. Constrained by its inherent principles, traditional display technologies struggle to achieve high pixel density and consistently face challenges related to the brightness and ambient reflection [11], [12]. Therefore, traditional display technologies fall certain short in meeting the requirements of near-eye display devices. The industry urgently needs novel display technologies to address the aforementioned issues.

Recently, researches on self-emissive displays such as organic light-emitting diodes (OLEDs) [13], [14], [15], micro light-emitting diodes (Micro-LEDs) [16], [17], [18], and quantum dot light-emitting diodes (QLEDs) [19], [20] have gained significant attention. These displays exhibit unprecedented application potential owing to the high brightness and contrast. The primary advantage of self-emissive displays lies in their independence from a backlight. By simply assembling a self-emissive display with the imaging lens group, the generated light can be directly used for projection engine and further coupled into the combiners, eliminating the need for complex and cumbersome relay optics [21], [22], [23], [24], [25]. Consequently, this significantly reduces the system volume and weight. Furthermore, self-emissive displays can independently emit light at each pixel, achieving higher contrast, more vibrant colors, and faster response time. This represents a qualitative leap in image quality and

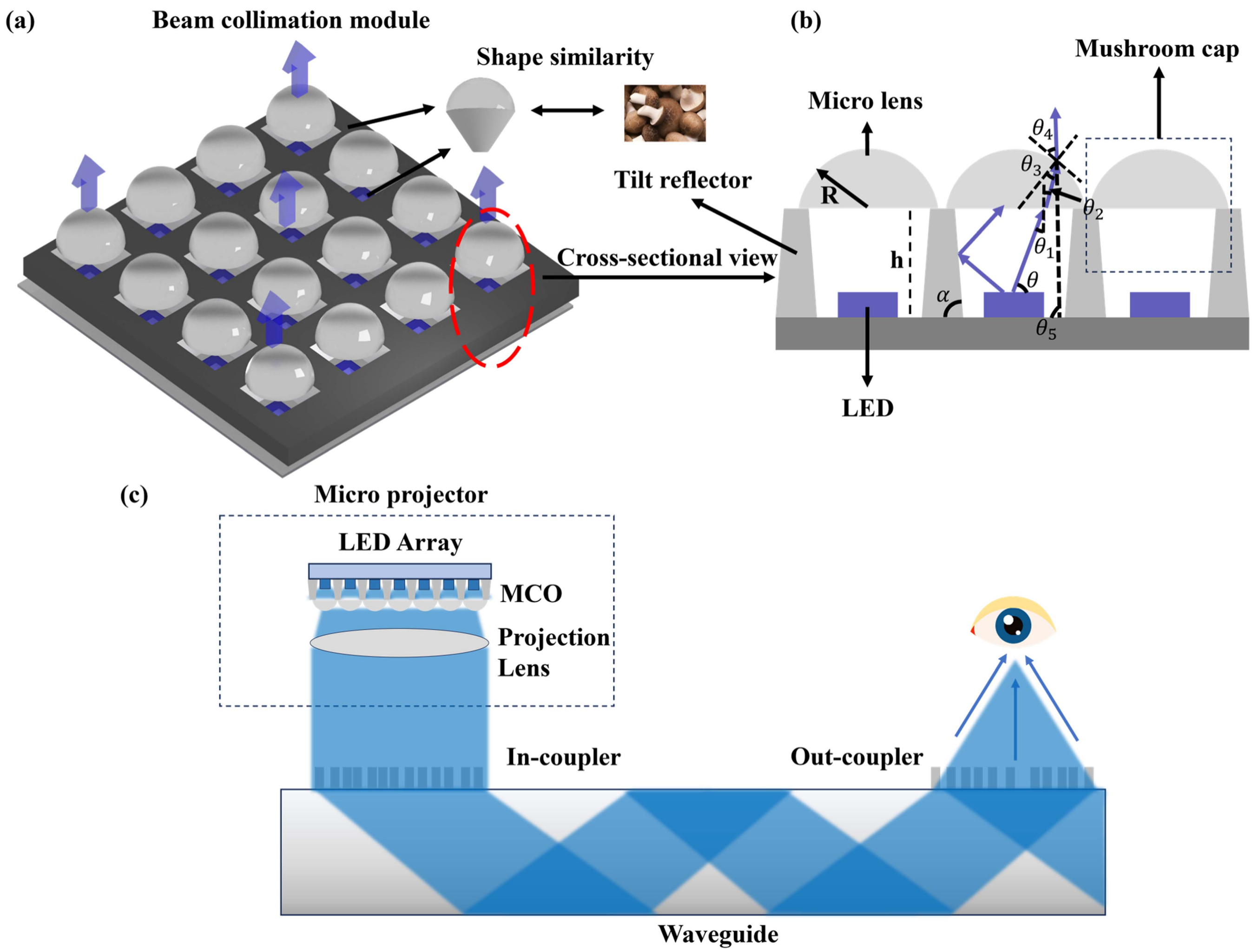

Fig. 1. (a) Schematic of the collimated LED array encapsulated with the MCO. (b) Cross-sectional view and the typical optical path of the LED array. (c) Schematic diagram of the working principle of an optical waveguide based near-eye display engine.

display performance [26], [27], [28], [29]. These advantages and characteristics make self-emissive light sources perfectly suited to meet the requirements of near-eye display devices, positioning them as the optimal breakthrough for the new era of display technology.

Current near-eye displays typically have brightness levels ranging from 1000 to 3000 nits. It is estimated that the ambient contrast ratio should be at least 10:1 for excellent readability. Indoor ambient brightness typically ranges around 150 nits, while outdoor ambient brightness can reach up to 3000 nits on a sunny day. In comparison, current near-eye display devices still have a significant shortfall in brightness [23]. Micro-LED technology offers a notable advantage in providing high brightness levels, having already achieved brightness levels in the hundreds of thousands of nits. Micro-LED displays can even provide brightness levels exceeding 3000000 nits. Therefore, compared to OLED and QLED technologies, Micro-LED technology has unparalleled advantages in near-eye display applications [26], [27], [28], [29].

However, it is noteworthy that despite the mentioned advantages of self-emissive light sources, they also face challenges related to light utilization efficiency. According to Lambert's cosine law, the emission angle of self-emissive light sources can reach approximately $\pm 60°$, while the actual usable emission area for each pixel is less than $\pm 30°$. This implies that these light sources generate a significant amount of "unused" light, which, without special treatment, cannot be utilized for the projection engine of near-eye displays and may cause crosstalk interference with other pixels [30], [31], [32], [33], [34]. Near-eye display engines typically consist of a collimated light source, a projection lens group, and a combiner [24], [25]. The light source and the projection lens together form the optical projection engine, while the combiner allows the user to see virtual images in the real world. Currently, the most promising combiner is the waveguide [6], [25]. In a typical waveguide, the image light first enters a glass plate through an in-coupler, then undergoes total internal reflection within the plate, and finally is projected onto the eye through an out-coupler at the other end, as shown in Fig. 1(c) [30], [31]. The in-coupler is sensitive to the angle of the light, and uncollimated light may affect the final image quality and field of view (FOV), thus requiring collimation of the light source [1], [25], [29].

Common collimation methods include the freeform curved lenses [41], reflectors [42], holographic optical elements [43], etc. Nevertheless, these methods consistently achieve collimation by treating the display panel as a surface source [32]. Therefore, it is necessary to implement pixel-level collimation for self-emissive light sources, restricting their emission angles and enhancing their luminous efficiency to better align with the requirements of near-eye display devices. Collimation methods for a single pixel primarily utilize lens array [36], while others have proposed the use of metasurfaces for collimation [44], as well as the techniques involving photonic crystals [45] and resonant cavities [46]. Potential issues include a high reliance on incident light and challenges in precise processing.

As shown in Fig. 1(a), inspired by the appearance of "mushroom cap", this paper introduces a novel collimated LED array structure with the encapsulation of mushroom-cap optical (MCO) units. This structure achieves LED pixel-level collimation and consists of two parts: the lower portion is a tilt reflector, and the upper portion is a hemispherical micro-lens. The tilt reflector reflects the aforementioned "unused" light, guiding it into the micro-lens. As a result, almost all light emitted from the LED pixel can be collimated by the micro-lens. The MCO structure significantly enhances light intensity, restricting the full width at half maximum (FWHM) within a quite small angular range, effectively avoiding crosstalk with other pixels.

The structural arrangement of this paper is as follows: Section II elaborates on the design principles of the MCO structure, determining optimal parameters for each component through simulation. This aims to provide theoretical guidance for subsequent experiments and applications. Section III validates the collimation performance and projection effects of the device through experiments. Finally, Section IV summarizes the main conclusions of the study and provides prospects for its application in near-eye display devices.

II. Design and Simulation

A. Design Principle

In order to streamline the calculation process for the MCO, the point light source approximation method is employed as the assumption. Leveraging geometric relationships, we can readily derive the interrelations among various angles according to Fig. 1(b).

$$\begin{cases} \theta_1 = \frac{\pi}{2} - \theta \\ \theta_2 = \arcsin \frac{\sin\theta_1}{n} \\ \theta_3 = \arcsin \frac{h\cdot\cos\theta_2}{R\cdot\tan\theta} \\ \theta_4 = \arcsin\left(n\cdot\sin\theta_3\right) \\ \theta_5 = \frac{\pi}{2} + \theta_2 + \theta_3 - \theta_4 \end{cases} \tag{1}$$

where n is the refractive index of micro-lens, R is the radius of the micro-lens, h is the length of the tilt reflector, θ denotes the angle with the horizontal plane when the light exits, θ_5 represents the final angle of the emitted light with respect to the horizontal plane. Obviously, the ultimate emission angle is solely dependent on these parameters along with the initial angle emitted from the LED.

Similarly, the angles of light emitted after reflection by the tilt reflector can be determined through geometric relationships.

$$\begin{cases} \theta_1^* = 2\alpha - \theta - \frac{\pi}{2} \\ \theta_2^* = \arcsin \frac{\sin\theta_1^*}{n} \\ \theta_3^* = \arcsin \frac{R - \left[\frac{h}{\tan\alpha} - \frac{r\cdot\sin\theta}{\sin(\alpha-\theta)}\right]\frac{\sin(\alpha-\theta)}{\sin(2\alpha-\theta)}}{R\cdot\cos\theta_2^*} \\ \theta_4^* = \arcsin\left(n\cdot\sin\theta_3^*\right) \\ \theta_5^* = \frac{\pi}{2} - \theta_2^* + \theta_3^* - \theta_4^* \end{cases} \tag{2}$$

In the above formula, α denotes the angle between the tilt reflector and the horizontal plane. θ_5^* denotes the angle between the light reflected by the tilt reflector and then collimated by the micro-lens and the horizontal plane. And the rest of the parameters with an asterisk correspond to (1).

To gain further insights into the impact of various structural parameters on the collimation performance, a three-dimensional Monte Carlo ray-tracing method is introduced. Systematically, the brightness enhancement and corresponding FWHM characteristics of the MCO are evaluated. During the simulation, considering practical situations, the light source volume was set to 20 μm $\times$ 15 μm $\times$ 5 μm, the pixel pitch was set to 80 μm, and the refractive index of the micro-lens was respectively set to 1.5. The initial height and tilt angle of the tilt reflector were set to 30 μm and 55° to comprehensively consider the impact of different parameter combinations. This helps us gain a more comprehensive understanding of the performance characteristics of the MCO.

B. Analysis on the Micro-Lens Size

In the simulation, the distance between the micro-lens and the light source were set to 30 μm, obtaining results as shown in Fig. 2(a). As depicted, we conducted simulations on the micro-lens radius within the range of 15 to 40 μm, discussing the impact of the radius on collimation performance.

With the continuous increase in the micro-lens radius, the maximum light intensity significantly improves. The light flux within $\pm 20°$ also increases, and during this process, the FWHM steadily decreases. Except for the light flux within $\pm 20°$, the optimal values for the other two indicators appear when the micro-lens radius is 40 μm. At the micro-lens radius of 40 μm, the maximum light intensity can reach 14 times that of the untreated LED, which is seven times that of a micro- lens radius of 15 μm. The FWHM is only $\pm 11.5°$, and the light flux within $\pm 20°$ can reach 4.8 times that of the untreated case.

Impressively, the MCO can achieve excellent collimation for the incoming Lambertian light. It can be considered that with the increase in the micro-lens radius, the collimation effect of the MCO improves. Therefore, the aperture of the micro-lens should be as close as possible to the pixel pitch to achieve better collimation effects.

C. Analysis on the Micro-Lens Position

The height of micro-lens placement has a great influence on the collimation performance. The micro-lens with the optimal radius of 40 μm is used for analysis. As shown in Fig. 2(b), the

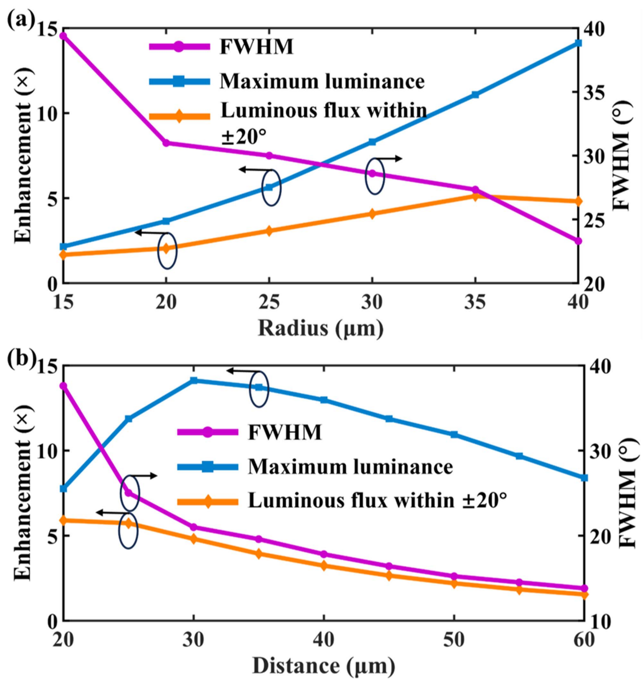

Fig. 2. Maximum light intensity, FWHM, and light flux within ±20° corresponding to different micro-lens radius at the same placement height. (b) Maximum light intensity, FWHM, and light flux within ±20° corresponding to different micro-lens placement heights at the same micro-lens radius.

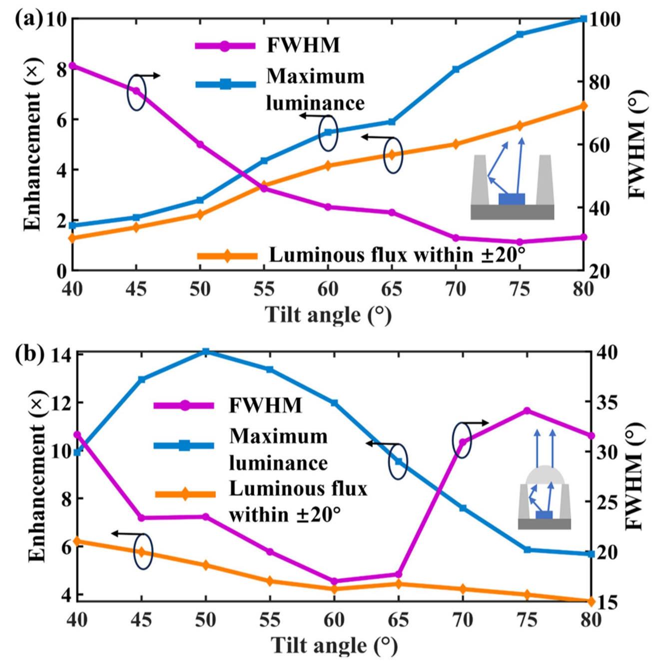

Fig. 3. (a) Maximum light intensity, FWHM, and light flux within ±20° corresponding to different tilt angles of the tilt reflector for the same aperture size. (b) Influence of different tilt angles of the tilt reflector on the collimation performance of MCO.

micro-lens placement height within the range of 20 to 60 μm are simulated.

With the increase in height, the maximum light intensity shows a trend of first increasing and then decreasing. At the distance of 30 μm from the LED, the maximum light intensity reaches its peak, being 14 times that of the untreated case. The FWHM steadily decreases with the increase in micro-lens placement height, and the light flux within ±20° follows the same trend. Since these three indicators are crucial for the final collimation effect, a micro-lens distance of 35 μm from the LED is the most suitable after comprehensive consideration. At this height, the maximum light intensity is 13.7 times that of the untreated case, while the FWHM is only ±9.8°, and the light flux within ±20° increases to 3.94 times that of the untreated case. In the case of this LED, the optimal collimation effect can be achieved by positioning a micro-lens with a 40 μm radius at a distance of 35 μm.

D. Design of Tilt Reflector

The main parameters of the tilt reflector include length, tilt angle, and aperture size. Since the aperture of the tilt reflector must match the micro-lens diameter, the tilt angle and length are entirely correlated. That means the larger the tilt angle is, the longer the length is. Therefore, the influence of the tilt angle on collimation performance with a fixed aperture is emphasized here.

From Fig. 3(a), it is evident that using only the tilt reflector already has a certain degree of collimation. As the tilt angle increases, both the maximum light intensity and the light flux within ±20° show an increasing trend, while the FWHM exhibits a gradual decrease. However, it is worth noting that when using only the tilt reflector, apart from the light flux within the ±20° range, this specific indicator is relatively superior to the MCO, the other two indicators differ significantly.

E. Design of the MCO

After separately discussing the optimal parameters for the micro-lens and tilt reflector, this section will explore the best parameters for their combination as the MCO. The micro-lens radius is fixed at 40 μm, so the primary consideration is the tilt angle of the tilt reflector's impact on the MCO. As shown in Fig. 3(b), it is observed that the FWHM tends to decrease as the tilt angle increases up to 60°. The maximum light intensity shows a trend of initially increasing and then decreasing, reaching its peak at a tilt angle of 50°, while the light flux within ±20° gradually decreases with increasing tilt angle. Considering all three indicators, we can conclude that the optimal range for the tilt angle is between 45° and 65°.

The trend of maximum light intensity in Fig. 3(b) is similar to the trend after 30 μm in Fig. 2(b). The length of the tilt reflector for a tilt angle of 50° is approximately 31.5 μm, close to 30 μm. Therefore, it can be considered that the gain in maximum light intensity for the MCO is mainly provided by the micro-lens. Similarly, before the tilt angle of 60°, the FWHM remains at a relatively low value, indicating the influence of the micro-lens.

F. Comprehensive Discussion on MCO Parameters

To determine the optimal parameter intervals for MCO, we conducted tests with a step size of 5 μm, ranging the radius from 15 to 40 μm and the distance from 15 to 60 μm. The

TABLE I
EFFECT OF DIFFERENT RADII AND DISTANCES OF MCO ON FWHM

Radius (μm) \ Distance (μm)	20	25	30	35	40	45	50	55	60
15	41.33°	46.56°	58.44°	66.68°	47.44°	65.32°	67°	67.25°	67.131°
20	37.55°	32.25°	31.18°	40.37°	49.69°	51.99°	51.15°	52.25°	52.56°
25	34.03°	29.8°	25.67°	25°	27.35°	36.86°	41.39°	42.82°	42.96°
30	30.42°	27.5°	24.41°	21.97°	20.93°	25.11°	28.58°	36.1°	35.96°
35	31°	24.89°	22.9°	21°	19.1°	17.3°	18.95°	24.36°	28.9°
40	38°	24.8°	21°	19.7°	18°	16.5°	**15.6°**	16.43°	18.7°

TABLE II
EFFECT OF DIFFERENT RADII AND DISTANCES OF MCO ON NORMALIZED MAXIMUM LIGHT INTENSITY

Radius (μm) \ Distance (μm)	20	25	30	35	40	45	50	55	60
15	0.15	0.14	0.13	0.12	0.12	0.12	0.11	0.11	0.12
20	0.26	0.25	0.23	0.21	0.2	0.18	0.18	0.17	0.17
25	0.42	0.4	0.38	0.34	0.31	0.29	0.26	0.26	0.25
30	0.59	0.57	0.56	0.51	0.47	0.42	0.4	0.36	0.35
35	0.64	0.78	0.77	0.74	0.68	0.62	0.54	0.52	0.48
40	0.53	0.86	**1**	0.98	0.94	0.87	0.79	0.68	0.65

TABLE III
EFFECT OF DIFFERENT RADII AND DISTANCES OF MCO ON NORMALIZED LUMINOUS FLUX WITHIN ±20°

Radius (μm) \ Distance (μm)	20	25	30	35	40	45	50	55	60
15	0.3	0.25	0.23	0.23	0.24	0.24	0.25	0.25	0.25
20	0.51	0.39	0.34	0.32	0.34	0.35	0.35	0.35	0.37
25	0.72	0.56	0.44	0.44	0.44	0.45	0.45	0.45	0.48
30	0.87	0.72	0.58	0.52	0.54	0.56	0.56	0.55	0.56
35	0.96	0.86	0.73	0.66	0.61	0.62	0.65	0.66	0.66
40	**1**	0.99	0.86	0.77	0.7	0.68	0.66	0.69	0.75

detailed results are presented in Tables I–III. Clearly, the MCO with a radius of 40 μm consistently outperforms in all three metrics. Additionally, the impact of MCO with different radii on collimation exhibits a similar trend: the maximum light intensity increases initially and then decreases, FWHM decreases initially and then increases, while the light flux within $\pm 20°$ increases initially and then decreases. Overall, the MCO with a radius of 40 μm demonstrates excellent collimation performance within the range of 25 to 50 μm from the light source. When converted to tilt angles, it corresponds to approximately 42° to 62°, which closely aligns with the results in Fig. 3(b). Therefore, the optimal parameter range for this design can be determined as a micro-lens radius of 40 μm and a tilt reflector tilt angle between 42° to 62°.

Since the illumination uniformity of the micro projector engine is crucial for the imaging of near-eye display. As shown

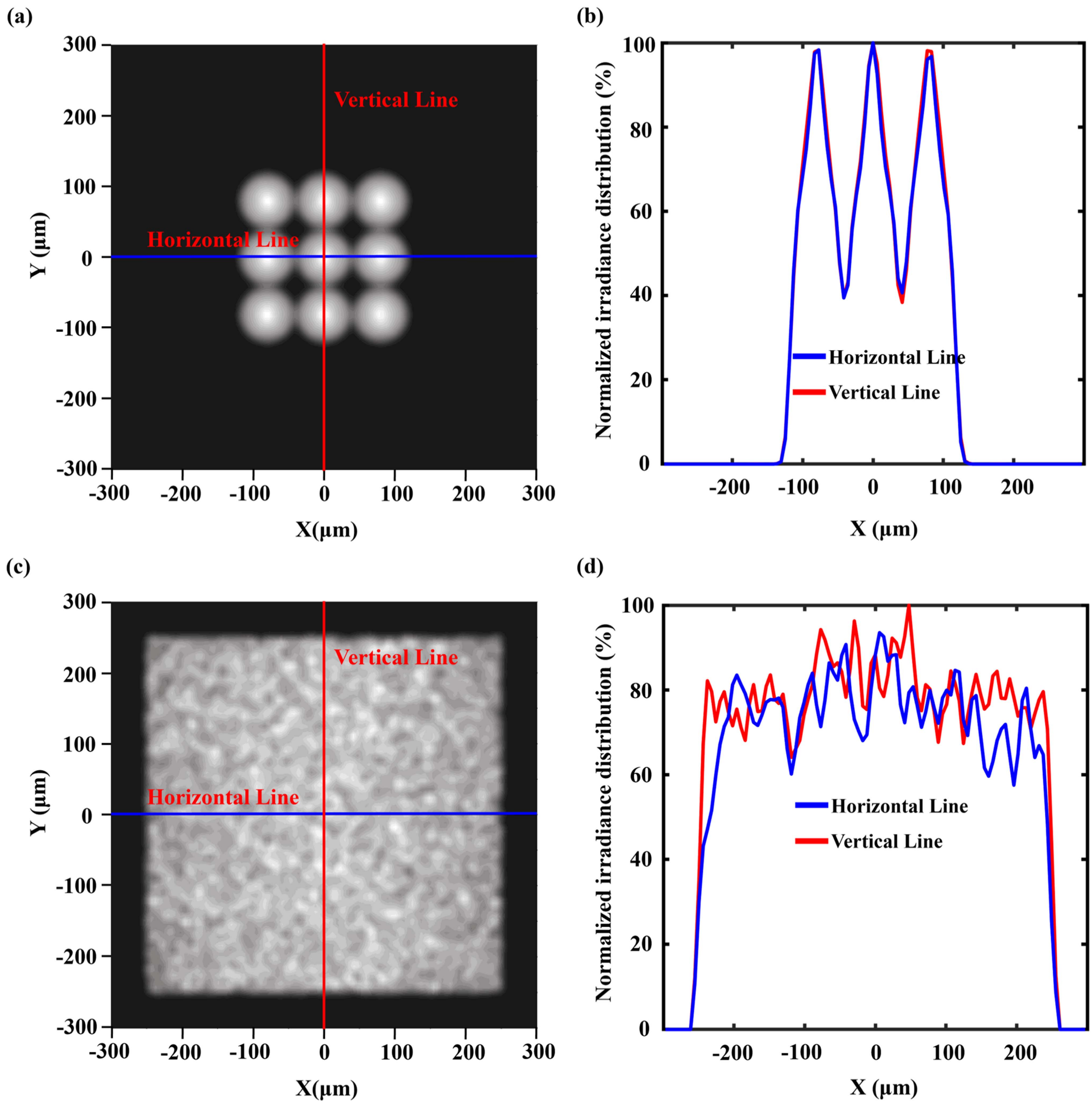

Fig. 4. (a) Homogeneous rectangular illumination at a distance of 10μm from the light source; (b) Normalized irradiance distribution along the reference line in the rectangular illumination area at a distance of 10 μm from the light source; (c) Homogeneous rectangular illumination at a distance of 3000 μm from the light source; (d) Normalized irradiance distribution along the reference line in the rectangular illumination area at a distance of 3000 μm from the light source.

in the Fig. 4, we tested the illuminance at distances of 10 μm and 3000 μm from the light source using the MCO with a tilt angle of 50°. Fig. 4(a) and (b) illustrates the illuminance distribution at a distance of 10 μm from the light source, while Fig. 4(c) and (d) depicts the illuminance distribution at a distance of 3000 μm from the light source. At the position 10 μm away from the light source, it can be considered as closely adjacent to the source. From Fig. 4(b), it is observed that the illuminance at the pixel center remains relatively consistent, and the boundaries between different pixels are clearly defined. Therefore, as a self-luminous display panel, its illuminance performance should be acceptable. At a distance of 3000 μm from the light source, it can be regarded as an application scenario of illumination for a non-self-luminous micro-display panel. In this case, the overall illuminance distribution appears quite uniform, as can be seen in Fig. 4(d). Thus, considering the above two sets of data collectively, we can conclude that whether used as a self-luminous display panel or an illumination light source, coupled with MCO, it can achieve outstanding illuminance distribution effects.

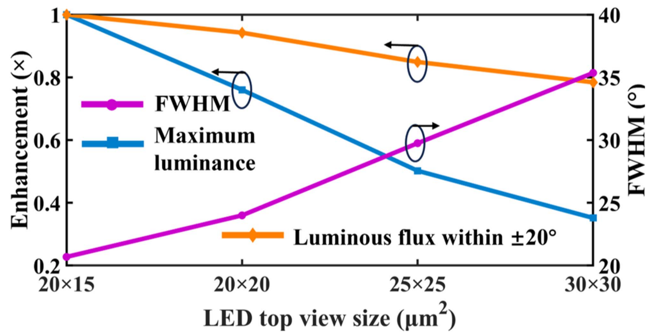

Fig. 5. Impact of LED size on the efficiency of MCO.

We also discussed the impact of LED size on the efficiency of MCO, and the results are presented in Fig. 5. The trends of the three datasets are quite apparent, showing a continuous decrease as the LED size increases. Therefore, it can be inferred that the efficiency of MCO increases with a higher ratio of MCO radius to LED size.

G. Comparison Between Traditional Black Matrix and MCO

In traditional LED designs, micro-lenses are often paired with a black matrix to achieve collimation. The black matrix effectively absorbs stray light, preventing light crosstalk between pixels, while micro-lenses are used for collimation. However, this also implies a decrease in light utilization efficiency. Consequently, the anisotropic backlight units could be a potential solution to replace black matrices [47]. Our proposed MCO can well replace the traditional black matrix, because the light absorbed by the black matrix can be effectively utilized through reflection. Here, the tilt angle of the tilt reflector represents its length, and their efficiency is compared with the traditional black matrix at the same height.

Based on the analysis in Section II-E, we have determined that the optimal efficiency of MCO occurs at tilt angles between 45° and 60°. Therefore, in this section, MCOs with tilt angles of 50°, 55°, and 60° will be selected and compared with the black matrix at the same height.

As shown in Fig. 6(a), comparing the maximum light intensity and FWHM, it can be observed that at the same height, the MCO has a slightly higher efficiency gain in maximum light intensity compared to the traditional black matrix, while the difference in FWHM is not significant. From Fig. 6(b), it is evident that within the ±20° range, the MCO's efficiency improvement is significantly superior to that of the traditional black matrix. The reasons for these phenomena are mainly due to the dominant role played by the micro-lens in collimation. At the same height, the light directly entering the micro-lens from the LED is the same, with the only difference being the light that cannot directly enter the micro-lens, i.e., those large angular rays. The traditional black matrix directly absorbs these rays, while the MCO's tilt reflector reflects this portion of light, allowing it to enter the micro-lens. After collimation, this portion of light is mainly distributed within the ±20° range. Therefore, although it may not significantly enhance the maximum light intensity, it can significantly increase the light flux within ±20°.

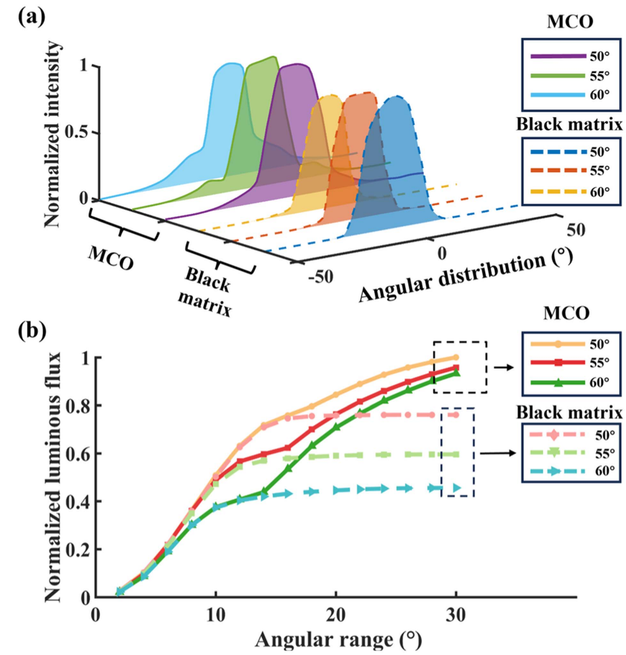

Fig. 6. (a) Comparison of the light intensity patterns between three different heights of MCO and the traditional black matrix. (b) Comparison of the light flux within the range between three different heights of MCO and the traditional black matrix.

III. Experiment

A projection prototype is established to evaluated the collimation performance via an amplification validation to the second section. The light intensity distribution of the LED array is measured using the SRC200 photometer from Everfine Optoelectronics. The LED array projectors with and without the MCO are shown in Fig. 7(a). From Fig. 7(b), each individual LED pixel has a size of 2 mm × 1.5 mm × 0.5 mm, and the pixel pitch is 8 mm. A 3 × 3 LED array is used for theoretical validation. Fig. 7(c) shows the fabricated MCO device. The actual projection prototype setup constructed on the optical platform consists of a LED light source array with MCO, a projection lens, and an imaging screen, as depicted in Fig. 7(d) and (e), showing the side and front views of the implemented projection apparatus. The projection lens used is provided by Azure Photonics, with a focal length of 37.5 mm and an f-number of 2.5. The horizontal field of view is 13.4°.

It can be observed that the maximum light intensity is increased tenfold when using the MCO compared to the original LED array. Additionally, FWHM is controlled to reflector, and the array combined with the MCO. After normalizing the obtained results, we obtained the results around ±10°, consistent with the simulation results in the second section. The tilt reflector alone also exhibits a certain collimation effect. From Fig. 7(f), it can be seen that the tilt reflector used in the experiment can constrain the FWHM to around ±30°, with the maximum

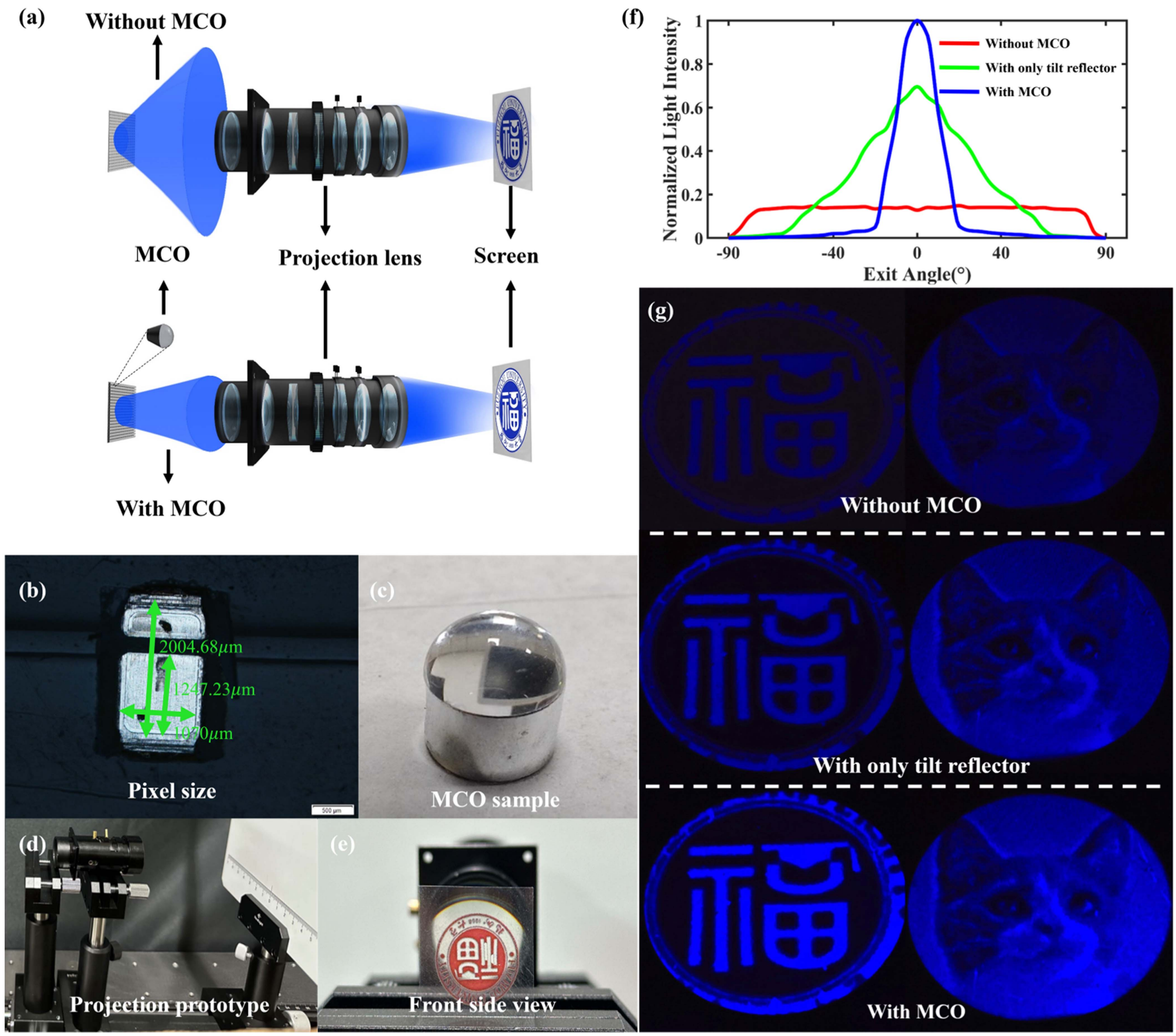

Fig. 7. (a) Schematic of the LED array projection engine with and without the MCO. (b) The LED light source used. (c) The fabricated MCO device. (d) Layout of projector prototype. (e) Front-side view of the projector. (f) The measured intensity distribution. (g) Actual projection effects of an untreated LED light source, tilt reflectors only, and MCO device.

light intensity approximately 70% of that with the MCO. This discrepancy is mainly attributed to the LED array undergoing uniform light treatment, resulting in emitted light that is not a standard Lambertian distribution.

Fig. 7(g) shows three imaging results, representing, from top to bottom, without the MCO, with only a tilt reflector, and with the MCO device. The initial projection effect of the LED projector without the MCO is poor, with very dim brightness, making it challenging to discern even the details of a cat. The use of the tilt reflector improves the projection effect compared to the untreated LED array, but still loses some image details due to insufficient brightness. It is evident that the LED projection engine after collimation with the MCO yields the brightest image with better projection effect, showcasing clear and detailed image details. Furthermore, it can be observed that the uniformity of the overall imaging is remarkably excellent.

IV. Conclusion

To meet the demands of near-eye displays [48], [49], this paper proposes a collimated LED array enlightened by the "mushroom cap" for near-eye display projection engines. Encapsulated in this manner, the FWHM of the LED array can be effectively controlled within the range of $\pm 10°$, resulting in a significant enhancement of central light intensity, and a notable increase in light flux within $\pm 20°$. Through the prototype establishment and experimental validation, our findings demonstrate that the LED light source array after collimation with the MCO achieves better and brighter imaging. In comparison with other collimation methods, the MCO exhibits significant improvements in one or more metrics. It is believed that the integration of MCO with LED projection engine can effectively achieve the high brightness required for near-eye display devices.

References

[1] J. Xiong, E.-L. Hsiang, Z. He, T. Zhan, and S.-T. Wu, "Augmented reality and virtual reality displays: Emerging technologies and future perspectives," *Light: Sci. Appl.*, vol. 10, no. 1, Oct. 2021, Art. no. 216, doi: 10.1038/s41377-021-00658-8.

[2] L. Mi et al., "Design of lensless retinal scanning display with diffractive optical element," *Opt. Exp.*, vol. 27, no, no. 15, pp. 20493–20507, Jul. 2019, doi: 10.1364/OE.27.020493.

[3] J. Chen et al., "Design of foveated contact lens display for augmented reality," *Opt. Exp.*, vol. 27, no. 26, pp. 38204–38219, Dec. 2019, doi: 10.1364/OE.381200.

[4] C. P. Chen et al., "Near-eye display with a triple-channel waveguide for metaverse," *Opt. Exp.*, vol. 30, no. 17, pp. 31256–31266, Aug. 2022, doi: 10.1364/OE.470299.

[5] N. Xi et al., "Implantable metaverse with retinal prostheses and bionic vision processing," *Opt. Exp.*, vol. 31, no. 2, pp. 1079–1091, Jan. 2023, doi: 10.1364/OE.478516.

[6] C. P. Chen et al., "Quad-channel waveguide-based near-eye display for metaverse," *Displays*, vol. 81, Nov. 2023, Art. no. 102582, doi: 10.1016/j.displa.2023.102582.

[7] B. C. Kress, *Optical Architectures for Augmented-, Virtual-, and Mixed-Reality Headsets*. Bellingham, WA, USA: SPIE, 2020.

[8] C. P. Chen, C. G. Jhun, T.-H. Yoon, and J. C. Kim, "Viewing angle switching of tristate liquid crystal display," *Jpn. J. Appl. Phys.*, vol. 46, no. 27, pp. L676–L678, Jul. 2007, doi: 10.1143/JJAP.46.L676.

[9] C. P. Chen et al., "Crosstalk-free dual-view liquid crystal display using patterned E-type polarizer," *Appl. Opt.*, vol. 56, no. 3, pp. 380–384, Jan. 2017, doi: 10.1364/AO.56.000380.

[10] B. S. Bae et al., "Dual structure of cholesteric liquid crystal device for high reflectance," *Electron. Mater. Lett.*, vol. 9, no. 6, pp. 735–740, Nov. 2013, doi: 10.1007/s13391-013-3122-2.

[11] C. P. Chen et al., "Transmissive interferometric display with single-layer Fabry-Pérot filter," *J. Disp. Technol.*, vol. 11, no. 9, pp. 715–719, May 2015, doi: 10.1109/JDT.2015.2432111.

[12] H.-W. Chen, J.-H. Lee, B.-Y. Lin, S. Chen, and S.-T. Wu, "Liquid crystal display and organic light-emitting diode display: Present status and future perspectives," *Light: Sci. Appl.*, vol. 7, Mar. 2018, Art. no. 17168, doi: 10.1038/lsa.2017.168.

[13] C. Chen et al., "Thin-film encapsulation for top-emitting organic light-emitting diode with inverted structure," *Chin. Opt. Lett.*, vol. 12, no. 2, Jan. 2014, Art. no. 022301, doi: 10.3788/COL201412.022301.

[14] X. Wei, H.-J. Yu, J. Cao, C. Jhun, and C.-P. Chen, "Efficient blue and white phosphorescent organic light-emitting diodes with a mixed host in emission layer," *Mol. Cryst. Liq. Cryst.*, vol. 651, no. 1, pp. 108–117, Oct. 2017, doi: 10.1080/09273948.2017.1338908.

[15] A. Salehi, X. Fu, D.-H. Shin, and F. So, "Recent advances in OLED optical design," *Adv. Funct. Mater.*, vol. 29, no. 15, Feb. 2019, Art. no. 1808803, doi: 10.1002/adfm.201808803.

[16] Y. Huang, E.-L. Hsiang, M.-Y. Deng, and S.-T. Wu, "Mini-LED, Micro-LED and OLED displays: Present status and future perspectives," *Light Sci Appl*, vol. 9, no. 1, Jun. 2020, Art. no. 1, doi: 10.1038/s41377-020-0341-9.

[17] T. Wu et al., "Mini-LED and micro-LED: Promising candidates for the next generation display technology," *Appl. Sci.*, vol. 8, no. 9, Sep. 2018, Art. no. 1557, doi: 10.3390/app8091557.

[18] X. Zhang et al., "Tripling light conversion efficiency of μLED displays by light recycling black matrix," *IEEE Photon. J.*, vol. 14, no. 2, Apr. 2022, Art. no. 7014207, doi: 10.1109/JPHOT.2022.3148241.

[19] J. Cao et al., "Bright hybrid white light-emitting quantum dot device with direct charge injection into quantum dot," *Chin. Phys. B*, vol. 25, no. 12, Oct. 2016, Art. no. 128502, doi: 10.1088/1674-1056/25/12/128502.

[20] J. Kim et al., "Ultrathin quantum dot display integrated with wearable electronics," *Adv. Mater.*, vol. 29, no. 38, Aug. 2017, Art. no. 1700217, doi: 10.1002/adma.201700217.

[21] C. P. Chen, L. Mi, W. Zhang, J. Ye, and G. Li, "Waveguide-based near-eye display with dual-channel exit pupil expander," *Displays*, vol. 67, Feb. 2021, Art. no. 101998, doi: 10.1016/j.displa.2021.101998.

[22] D. Cheng et al., "Design and manufacture AR head-mounted displays: A review and outlook," *Light: Adv. Manuf.*, vol. 2, no. 3, pp. 350–369, Sep. 2021, doi: 10.37188/lam.2021.024.

[23] L. Deng et al., "Ambient contrast ratio of quantum-dot color-converted micro-LED displays," *Results Phys*, vol. 48, May 2023, Art. no. 106462, doi: 10.1016/j.rinp.2023.106462.

[24] Z. Liu et al., "Metasurface-enabled augmented reality display: A review," *Adv. Photon.*, vol. 5, no. 3, May 2023, Art. no. 034001, doi: 10.1117/1.AP.5.3.034001.

[25] Y. Ding et al., "Waveguide-based augmented reality displays: Perspectives and challenges," *eLight*, vol. 3, no. 1, Dec. 2023, Art. no. 24, doi: 10.1186/s43593-023-00057-z.

[26] Y. Liu et al., "Omnidirectional color shift suppression of full-color micro-LED displays with enhanced light extraction efficiency," *Opt. Lett.*, vol. 48, no. 7, pp. 1650–1653, Apr. 2023, doi: 10.1364/OL.486014.

[27] Z. Du et al., "Efficiency improvement of GaN-based micro-light-emitting diodes embedded with Ag NPs into a periodic arrangement of nano-hole channel structure by ultra close range localized surface plasmon coupling," *Nanotechnology*, vol. 33, no. 49, Sep. 2022, Art. no. 495202, doi: 10.1088/1361-6528/ac8f98.

[28] Z. Du et al., "Localized surface plasmon coupling nanorods with graphene as a transparent conductive electrode for micro light-emitting diodes," *IEEE Electr. Device Lett.*, vol. 43, no. 12, pp. 2133–2136, Dec. 2022, doi: 10.1109/LED.2022.3217167.

[29] E. Chen et al., "Metamaterials for light extraction and shaping of micro-scale light-emitting diodes: From the perspective of one-dimensional and two-dimensional photonic crystals," *Opt. Exp.*, vol. 31, no. 11, pp. 18210–18226, May 2023, doi: 10.1364/OE.489598.

[30] C. Pan et al., "Design of a high-performance in-coupling grating using differential evolution algorithm for waveguide display," *Opt. Exp.*, vol. 26, no. 20, pp. 26646–26662, Oct. 2018, doi: 10.1364/OE.26.026646.

[31] D. Cheng, Y. Wang, C. Xu, W. Song, and G. Jin, "Design of an ultra-thin near-eye display with geometrical waveguide and freeform optics," *Opt. Exp.*, vol. 22, no. 17, pp. 20705–20719, Aug. 2014, doi: 10.1364/OE.22.020705.

[32] Y. Li et al., "Highly efficient and ultra-compact micro-LED pico-projector based on a microlens array," *J. Soc. Inf. Disp.*, vol. 31, no. 7, pp. 483–493, 2023, doi: 10.1002/jsid.1215.

[33] H. Jiang et al., "Design of self-luminous pico-projection optical engine based on a quantum-dot color converted micro-LED," *Proc. SPIE*, vol. 12448, Nov. 2022, Art. no. 1244815, doi: 10.1117/12.2638380.

[34] H. Jiang et al., "Projection optical engine design based on tri-color LEDs and digital light processing technology," *Appl. Opt.*, vol. 60, no. 23, pp. 6971–6977, Aug. 2021, doi: 10.1364/AO.432355.

[35] T. Jung, J. H. Choi, S. H. Jang, and S. J. Han, "Review of micro-light-emitting-diode technology for micro-display applications," *Dig. Tech. Pap. SID Int. Symp.*, vol. 50, no. 1, pp. 442–446, May 2019, doi: 10.1002/sdtp.12951.

[36] W. C. Chong et al., "Low optical crosstalk micro-LED micro-display with semi-sphere micro-lens for light collimation," *Dig. Tech. Pap. SID Int. Symp.*, vol. 49, no. S1, pp. 339–342, Nov. 2018, doi: 10.1002/sdtp.12720.

[37] E. Chen, R. Wu, and T. Guo, "Design a freeform microlens array module for any arbitrary-shape collimated beam shaping and color mixing," *Opt. Commun.*, vol. 321, pp. 78–85, Jun. 2014, doi: 10.1016/j.optcom.2014.01.032.

[38] X. Hu et al., "Design of inclined omni-directional reflector for sidewall-emission-free micro-scale light-emitting diodes," *Opt. Laser Technol.*, vol. 154, Jun. 2022, Art. no. 108335, doi: 10.1016/j.optlastec.2022.108335.

[39] H. Wang et al., "Role of surface microstructure and shape on light extraction efficiency enhancement of GaN micro-LEDs: A numerical simulation study," *Displays*, vol. 73, Jul. 2022, Art. no. 102172, doi: 10.1016/j.displa.2022.102172.

[40] B. Demory et al., "Integrated parabolic nanolenses on MicroLED color pixels," *Nanotechnology*, vol. 29, no. 16, Feb. 2018, Art. no. 165201, doi: 10.1088/1361-6528/aaac5f.

[41] L. Wang, K. Qian, and Y. Luo, "Discontinuous free-form lens design for prescribed irradiance," *Appl. Opt.*, vol. 46, no. 18, pp. 3716–3723, Jun. 2007, doi: 10.1364/AO.46.003716.

[42] S. Thiele, T. Gissibl, H. Giessen, and A. M. Herkommer, "Ultra-compact on-chip LED collimation optics by 3D femtosecond direct laser writing," *Opt. Lett.*, vol. 41, no. 13, pp. 3029–3032, Jul. 2016, doi: 10.1364/OL.41.003029.

[43] Y. Xiong et al., "Coherent backlight system for flat-panel holographic 3D display," *Opt. Commun.*, vol. 296, pp. 41–46, Feb. 2013, doi: 10.1016/j.optcom.2013.01.045.

[44] Z. Fan et al., "Highly collimating micro-LED projection source enabled by metasurface," *Proc. SPIE*, vol. 12964, Dec. 2023, Art. no. 1296407, doi: 10.1117/12.3005257.

[45] T. Wang et al., "GaN-on-Si micro resonant-cavity light-emitting diodes with dielectric and metal mirrors," *Opt. Mater.*, vol. 143, Sep. 2023, Art. no. 114096, doi: 10.1016/j.optmat.2023.114096.

[46] J. Huang et al., "GaN-based resonant cavity micro-LEDs for AR application," *Appl. Phys. Lett.*, vol. 121, no. 20, Nov. 2022, Art. no. 201104, doi: 10.1063/5.0117568.

[47] C.-J. Zhao, Z.-D. Guo, H. Deng, C.-N. Yang, and Y.-C. Bai, "Integral imaging three-dimensional display system with anisotropic backlight for the elimination of voxel aliasing and separation," *Opt. Exp.*, vol. 31, no. 18, pp. 29132–29144, Aug. 2023, doi: 10.1364/OE.498147.

[48] C. P. Chen et al., "Design of retinal projection displays enabling vision correction," *Opt. Exp.*, vol. 25, no. 23, pp. 28223–28235, Oct. 2017, doi: 10.1364/OE.25.028223.

[49] W. Zhang et al., "See-through near-eye display with built-in prescription and two-dimensional exit pupil expansion," *Appl. Sci.*, vol. 10, no. 11, Jun. 2020, Art. no. 3901, doi: 10.3390/app10113901.

Enguo Chen (Member, IEEE) received the Ph.D. degree in optical engineering from Zhejiang University, Zhejiang, China, in 2013. He visited the Hong Kong University of Science and Technology, Hong Kong, and University of Central Florida, Orlando, FL, USA, as a Research Scholar. He is currently a full Professor with Fuzhou University, Fuzhou, China, with a joint appointment as a distinguished research Fellow of Fujian Science & Technology Innovation Laboratory for Optoelectronic Information of China. Till now, his research has been funded by several grants from national or regional government, and he has also cooperated with several well-known display manufacturers. He has authored or coauthored more than 100 papers in academic journals and conference proceedings and owned more than 50 authorized Chinese invention patents. His research interests include the optical design of optical systems and emerging display technologies. He is the Member of OSA, SID, ACS, and Chinese Vacuum Society, and was the reviewer for more than 50 peer-reviewed journals and TPC Member for several academic conferences.

Ziming Yao received the B.S. degree in space science and technology from Xidian University, Xi'an, China. He is currently working toward the M.S. degree with the Fujian Science & Technology Innovation Laboratory for Optoelectronic Information of China, Fuzhou University, Fuzhou, China. His research focuses on full color micro LED display.

Zhengui Fan received the B.S. degree in electronic information engineering from the Fujian University of Technology, Fujian, China. He is currently working toward the M.S. degree with the Fujian Science & Technology Innovation Laboratory for Optoelectronic Information of China, Fuzhou University, Fuzhou, China. His research focuses on full-color micro-LED display.

Wenzong Lai received the M.S. degree in mechanical engineering from the Fujian University of Technology, Fujian, China. He is currently working toward the doctoral degree with the Fujian Science & Technology Innovation Laboratory for Optoelectronic Information of China, Fuzhou University, Fuzhou, China. His research focuses on full-color micro-LED display.

Tao Liang received the B.S. degree in Internet of Things engineering from Fuzhou University, Fuzhou, China. He is currently working toward the M.S. degree with the Fujian Science & Technology Innovation Laboratory for Optoelectronic Information of China, Fuzhou University. His research focuses on high-density micro-LED optical design.

Qun Yan (Member, IEEE) is national distinguished expert, authoritative scholar in the international display industry, and R&D Scientist. He has more than 40 journal publications, 28 conference presentations, and 40 patents in his professional career. He is currently devoted to the research and development of highly integrated semiconductor information display based on Micro-LED and interactive rich media technology. He is SID Fellow, Member of SID Global Executive Committee and SID Global Treasurer, Director of SID Beijing Chapter, and CEO of SID China. He is the Chair of Display Technology Training School Committee at SID. He was the recipient of the SID Special Recognition Award in 2013 and SID Fellow Award in 2017. He was the Chief Scientist for Changhong Electric Group and the Chief Research Scientist at Panasonic Plasma Display Laboratory of America Inc. He is currently full time distinguished Professor with Fuzhou University, Fuzhou, China He is also holding joint professorship as the doctoral supervisor with Xi'an Jiaotong University, Xi'an, China, and Southeast University, Nanjing, China.

Tailiang Guo received the M.S. degree in applied physics from Fuzhou University, Fuzhou, China, in 1986. He has authored or coauthored more than 200 papers on display technologies. His research interests include field emission display materials and devices, 3D display, printing electronics, and their applications.

Chao Ping Chen (Member, IEEE) received the Ph.D. degree in electronic engineering from Pusan National University, Busan, South Korea. He has authored or coauthored 62 SCI-indexed journal papers, eight EI-indexed/other journal papers, 86 international conference papers, 41 patent applications (issued: 22), and two software copyrights. According to Google Scholar, his publications have received a total of citations more than 1300 (h-index: 22). His research interests include the metaverse, augmented/virtual reality, biomimetic displays, wearable displays, and vision sciences. National research funding (number of grants: six): National Natural Science Foundation of China (key/regular/youth programs), Ministry of Science and Technology (973/863 programs), and National Development and Reform Commission (National Engineering Lab). National institution/organization positions: National Natural Science Foundation of China (grant reviewer), Ministry of Education (dissertation reviewer), National Virtual Reality Innovation Center (council member), and Ministry of Industry and Information Technology's World Conference on VR Industry (final-round judge). SCI journal editorship: Elsevier Optics and Lasers in Engineering IF = 4.6 (guest editor), Elsevier Displays IF = 4.3 (editor), Optica/OSA Optics Express IF = 3.8 (guest editor).